Department of Engineering Physics and Mathematics
Helsinki University of Technology
02150 Espoo, Finland

INFLUENCE OF ELECTROMAGNETIC ENVIRONMENT IN SINGLE TUNNEL JUNCTIONS

Jari Penttilä

Low Temperature Laboratory

Dissertation for the degree of Doctor of Science in Technology to
be presented with due permission for public examination
and debate in Auditorium F1 at the Helsinki University
of Technology on the 7th of April, at 12 noon.

Espoo 2001

Keywords: electron transport in mesoscopic systems, Josephson effects, Coulomb blockade

Abstract

In this Thesis, electron transport through single tunnel junction embedded in a dissipative environment was studied both in normal and superconducting state. High-voltage asymptotics of the current-voltage (IV) characteristics for small normal tunnel junctions and carbon nanotubes were studied experimentally. Power-law voltage tails of IV curve were detected when approaching the linear law $V = IR + e/2C$ at large voltages with the offset depending of the junction capacitance C.

The effect of environment is in fact a result of Johnson-Nyquist noise in the electric circuit. In our low temperature measurements, the power-law tails at high voltages are connected only with the quantum part of Johnson-Nyquist noise. Thus, detection of these tails in a good agreement with the quantum theory of environment is a rather unique verification of quantum zero-point fluctuations in macroscopic systems.

Our experimental conditions included the case of strong tunneling when the junction resistance R_T was less than the quantum resistance R_K. The strong-tunneling corrections to the environmental modes at high voltages can be simply incorporated by including the junction resistance R_T into the effective electric circuit for calculation of the quantum noise.

In the superconducting state, our experiments for the first time clearly confirm the existence of the dissipative phase transition in a single Josephson junction. In the transition, dissipation destroys the quantum mechanical band structure and restores the classical Josephson behavior of dynamics governed by the classical phase difference φ.

The observed phase diagram differed from that expected originally. The agreement with theory was achieved by taking into account that the position of the measured phase boundary is governed not only by intrinsic junction parameters, but also by the accuracy of voltage measurement. Our work is a strong demonstration of quantum effects in a single Josephson junction, especially, of the Josephson phase delocalization and the band picture of phase motion.

ISBN 951-22-5388-7

To Olli and Jaakko

Contents

1 Introduction

This Thesis reports experimental studies on ultrasmall single tunnel junctions, both superconducting and normal. We have performed detailed measurements on the effect of external dissipation on transport of Cooper pairs and normal electrons in single tunnel junctions. Ohmic damping which is inversely proportional to the parallel resistance R is obtained using high-resistance chromium strips as measurement leads. In the case of superconducting Josephson junction, weak damping ($R^{-1} < R_q^{-1} \approx (6.5\ \mathrm{k\Omega})^{-1}$) reveals the quantum mechanical band structure of phase of the superconducting order parameter. The band structure of Josephson junction is analogous to energy bands of Bloch electrons in solids, phase difference and quasicharge (φ, Q) playing the roles of coordinate and crystal momentum (x, p) of the Bloch electron. The motion of φ along the energy band causes a resistive zero-bias anomaly in current-voltage characteristics. As damping is increased, dissipation destroys the quantum mechanical band structure and restores the classical Josephson behavior of dynamics governed by the classical phase difference φ.

Normal tunnel junctions are investigated in the high voltage regime, where the resistive Cr leads turn into transmission lines with distributed resistance, inductance and capacitance. The Johnson-Nyquist noise in these leads affects the tunneling rate of electrons through the junction. The tunneling current can be calculated using well-established theory [P(E)-theory] and quantitative agreement with the measurement is found.

The experiments were carried out in the Low Temperature Laboratory during the period 1996-1999. Publications P1-P4 describe measurements on single Josephson junctions, which reveal the dissipative phase transition. This is the first systematic study covering the whole phase diagram. Publications P5-P6 deal with experiments on normal single junctions with emphasis on the effect of environment (*i.e.* measurement leads) on the current-voltage characteristics at large voltages. The same theoretical framework is employed also for transport in carbon nanotubes in P7. Some other fields of electron transport in mesoscopic scale are studied in publications P8-P10. In these publications, the sample has two tunnel junctions in series forming a so-called single electron transistor. In publication P8 the transistor is built of carbon nanotube, whereas in publications P9 and P10 the charge noise of two conventional metallic single electron transistors is investigated.

1.1 Coulomb blockade in normal tunnel junctions

A tunnel junction is formed between two metallic electrodes separated by a thin layer of oxide insulator, as illustrated in Fig. 1. At low enough temperatures, $k_B T \ll e^2/2C$, and in highly resistive circuit the electrons are localized on the junction capacitance C because once one electron has tunneled through the junction the others are blocked by

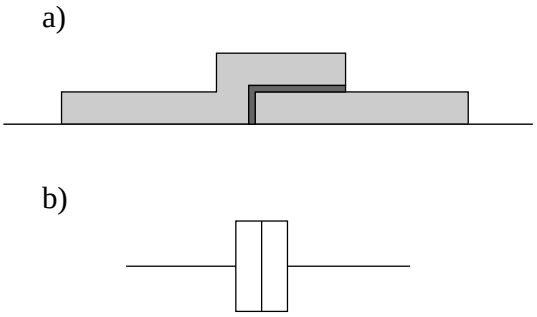

Figure 1: a) An overlap tunnel junction and, b) its symbol.

the energy barrier given by $e^2/2C$. Here $E_c = e^2/2C$ is the electrostatic charging energy of the capacitor C charged by an elementary charge e. The first evidence of charging effects were obtained already in the 1960's on granular films [1, 2, 3]. On these systems, a decrease of DC conductance at low bias voltages was observed. However, since the system consisted of irregular grains, no direct information about single junction properties was obtained. After the advent of modern lithographic techniques, ultra-small single tunnel junctions can be fabricated routinely. In these junctions C can be made as small as 10^{-15} F and the charging energy E_c corresponds to temperature of the order of 1 Kelvin. This has resulted in extensive theoretical and experimental studies on the effect of Coulomb blockade of tunneling since mid-1980's. (See e.g. [4], [5] and [6] for further references).

Lithography allows us to contact a mesoscopic tunnel junction (size 100×100 nm^2) to macroscopic measuring setups. Thus, the microscopic quantum-mechanical processes in the junction can be observed and controlled in a simple way. However, one must be careful since the macroscopic environment influences the behavior of the junction and thus the outcome of the measurements.

Let us now contact the single tunnel junction to a voltage source. In ideal voltage bias the tunneled charge is immediately removed from the junction and the only energy scale involved is eV, the work done by the voltage source. This results in a linear current-voltage relationship without Coulomb blockade. On the other hand, by adding a large resistor R in series with the voltage source we are slowly charging the junction capacitance with time constant RC until its voltage exceeds the charging energy ($V > e/2C$). At this point an electron can tunnel through the junction changing the capacitor charge by e and the process of slow charging continues (see the energy diagram of Fig. 2). This results in an offset in current-voltage characteristics given by $e/2C$. It is also worth to notice that the charging process involves correlation of subsequent tunneling events occurring with a fundamental frequency of $f_s = I/e$, also known as single-electron tunneling oscillations.

Two limiting cases of ideal voltage and current biases corresponding to environmental

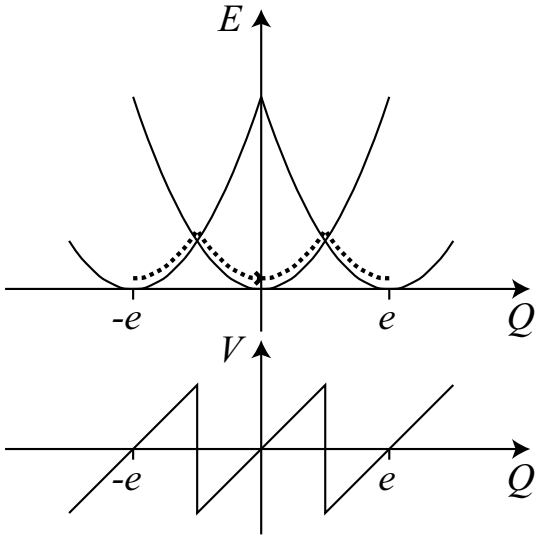

Figure 2: Upper: Energy diagram for a normal tunnel junction. At the degeneracy points two charge states (parabolas) have equal energy and tunneling between them is possible. Dashed line shows the adiabatic motion of the charge $\dot{q} = I$ for a current biased junction, with tunneling of a single electron at $-e/2, e/2, etc.$ The lower graph shows the junction voltage defined as $V = dE/dQ$. In the current biased case, for voltages $V < e/2C$ the junction does not conduct, $\dot{q}$=0.

impedances $Z(\omega) = 0$ and $Z(\omega) = R \to \infty$ are depicted in Fig. 3 in the limit of large tunneling resistance R_T of the junction. As the above discussion reveals, already a simple resistive environment strongly influences the current-voltage characteristics. In reality, the environment consists also of stray capacitances and inductances of the measurement leads. These components become more important at higher voltages across the junction. It was realized quite early [7] that the stray capacitance of the leads effectively shunts the junction already at the distance of a few tens of microns. This is why in subsequent experiments the junctions were surrounded by on-chip high-resistance thin film resistors (see e.g. [8]).

In usual perturbation theory [4, 9], one assumes that the tunneling resistance R_T is much larger than the quantum of resistance $R_K = h/e^2 = 25.8$ kΩ. This is to say that the charging energy E_c is much larger than the scale of quantum fluctuations given by $\sim \hbar/R_T C$. However, our samples are in the strong tunneling regime, where $R_T \sim R_K$ or even smaller. A question arises, is there a simple way to account for strong tunneling in the current-voltage curves of a single tunnel junction?

The effect of environmental fluctuations on the current-voltage characteristics on a

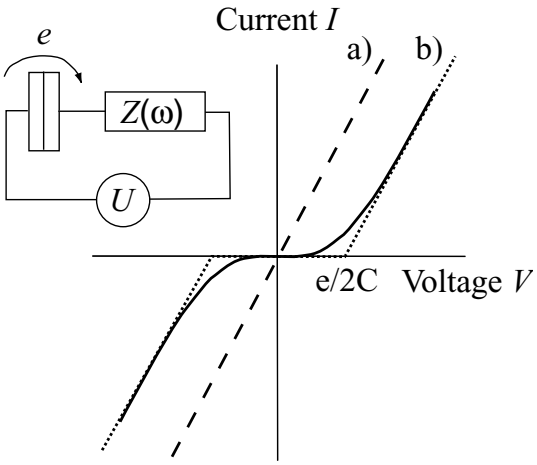

Figure 3: Ideal current-voltage characteristics for the circuit depicted in the inset. a) Dashed line: voltage bias $Z(\omega) \to 0$, b) dotted line: current bias $Z(\omega) = R \to \infty$. Solid curve shows a realistic curve with smoothing caused by finite temperature and finite impedance Z.

single normal tunnel junction as well as strong tunneling effects have been studied in Chapter 3 of this Thesis.

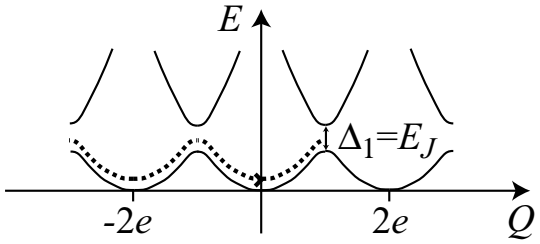

Figure 4: Two lowest energy bands of a Josephson junction with $E_J \ll E_c$. Supercurrent is realized as 2e-periodic motion along the lowest energy band. At low temperatures and currents, Zener tunneling across the gap Δ_1 is small. At small Q, the band is given by $E(Q) = Q^2/2C$, and the width of the band is $\Delta \approx e^2/2C$.

1.2 Superconducting tunnel junctions

In Josephson junctions we must consider tunneling of Cooper pairs. At the same time quasiparticle tunneling is reduced due to opening of the superconducting gap. Neglecting quasiparticles the Hamiltonian gets a simple form [10]

$$H = \frac{Q^2}{2C} - E_J \cos(\varphi), \tag{1}$$

where charge of the capacitor Q and phase difference of the condensate wave functions φ are conjugate variables analogous to the familiar pair coordinate - momentum for a particle [11]. Similarly, Eq. 1 determines the motion of a fictitious phase particle in a washboard potential with $2e$-periodic energy eigenvalues $E_n(Q)$ as a function of Q, also called quasicharge, Fig. 4 [7].

As already discussed in the context of current-biased normal tunnel junction, the current through the junction is blocked as long as the junction voltage is small. Remembering the uncertainty principle between phase and quasicharge, in this regime of Coulomb blockade for Cooper pair tunneling the quasicharge is fixed and phase difference fluctuates strongly. At finite currents, however, so-called Bloch oscillations occur with frequency $f_B = I/2e$ as the quasicharge travels along the lowest energy band as shown in Fig. 4.

An important requirement for the existence of Bloch energy bands is that the damping parameter should be low, $\alpha_s = R_q/R < 1$, where $R = Z(0)$ is the low frequency resistive part of the environmental impedance. Low damping allows quantum fluctuations (macroscopic quantum tunneling) of phase difference which are necessary for the energy bands to exist. On the other hand, large damping kills the fluctuations and locks the phase into one potential well of the washboard potential. This corresponds to a classical Josephson

behavior with supercurrent at zero voltage (for review, see [12]).

In our experiments, the effect of damping on the characteristics of a single Josephson junction is studied. We have mapped the transition between classical and quantum regimes briefly discussed above. This so-called dissipative phase transition is the topic of Chapter 4.

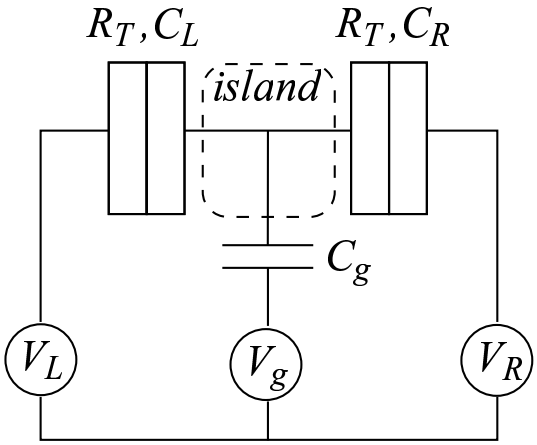

Figure 5: Schematic diagram of a single electron tunneling transistor (SET). An island is connected to the source and drain via tunnel junctions C_L and C_R. The gate is operated using a small capacitor C_g.

1.3 Multiple junction circuits

The effect of electromagnetic environment on electron tunneling can be substantially reduced by adding several junctions in series. The simplest example, the so-called single electron tunneling transistor (SET), consists of two junctions separating an island from the external leads (Fig. 5). Network analysis [13] shows that the effect of external impedance $Z(\omega)$ is reduced by a factor of $1/N^2$ for N similar junctions in series. Thus, the environment for circuits consisting of several tunnel junctions can be regarded as a low impedance one.

If the capacitances C_L, C_R, and C_g are small enough and the tunneling resistance R_T is large, the number of electrons n in the island is quantized due to Coulomb blockade at low temperatures. The relevant energy is again the charging energy $E_c = (ne - Q_g)^2/2C$, where C is the total capacitance of the island and $Q_g = C_g V_g$ is the gate charge. In the tunneling process, increasing the island charge from n to $n+1$, the charging energy changes

$$\Delta E_c(n, Q_g) = (n + \frac{1}{2} - \frac{Q_g}{e})\frac{e^2}{C}. \tag{2}$$

The energy difference and subsequently the tunneling rate across the transistor can thus be varied using a voltage source connected to the gate capacitance. This results in an e-periodic IV-curve as a function of Q_g. The dependence of IV curve on Q_g is used in electrometry to detect ultrasmall variations of electric charge. The best charge noise reported so far is $8{\cdot}10^{-6}\ e/\sqrt{\text{Hz}}$ at 10 Hz corresponding to roughly 30 $\hbar$ [14].

At low frequencies, the major problem in applying SET transistors in electrometry

is $1/f$ noise, which is caused by background charge variations due to trapping centers both in the vicinity of the island as well as in the tunnel barriers themselves. The effect of sample fabrication on $1/f$ noise was studied in P9, where two different substrates for SETs were compared. However, within our resolution no contribution could be assigned to the lithographic process.

Another source of noise could be fluctuations in tunnel resistance R_T. This was investigated in P10, where a bias reversal scheme was applied to average out the fluctuations in R_T. Compared with simple dc biasing we could deduce that the noise in the studied devices was true background noise and no contribution due to tunnel resistance was seen.

2 Experimental setup

This chapter is divided into two parts. In the first section the sample fabrication process consisting of lithography and metallization is discussed. The latter section describes the low-noise electrical measurement setup as well as cooling of the samples.

2.1 Sample fabrication

Nowadays, the suspended bridge technique developed by Dolan [15] is commonly used in nanofabrication. Using this technique, several layers of metals can be evaporated in an aligned fashion during the same vacuum cycle. The tunnel junction is formed by oxidizing the sample between two subsequent metallizations.

First of all, a (100) silicon wafer was covered by a bilayer resist. The more sensitive bottom layer (PMMA/MAA) provided the large undercut needed in the suspended bridge technique. Secondly, a thin layer of PMMA was spun on top in order to pattern narrow features ($\sim$ 100 nm). Table 1 summarizes the used recipes.

Table 1: Most of the samples were fabricated using the following recipe.

wafer	4-inch oxidized silicon wafer	
bottom layer	5.5 weight-% P(MMA/MAA) in acetic acid	2200 rpm (300 nm)
bake 1.5 hours at 160 °C		
top layer	3 weight-% PMMA in chlorobenzene	7000 rpm (140 nm)
bake 8 hours at 160 °C		
electron beam exposure at 40 kV		
1st developer	methyl ethyl ketone : ethanol (1:1)	15 s at 17 °C
2nd developer	methyl isobutyl ketone	60 s at 17 °C
rinse	isopropanol	ultrasonic bath

The patterning was accomplished by using electron beam lithography (See e.g. [16] for references). For that purpose we used a converted scanning electron microscope (JEOL JSM-6400) with NPGS pattern generation software by JC Nabity Lithography Systems, Inc. [17]. The accelerating voltage was 40 kV and the beam currents were 6 pA and 100 nA for writing narrowest lines and soldering pads, respectively. The minimum line width obtained was limited to about 50 nm due to the thickness of the resist. Using a thinner resist, line widths as small as 20 nm were obtained.

After patterning, the sample chip (about 4×8 mm^2, containing 1-3 samples) was developed during 10-15 s in solution of methyl ethyl ketone and ethanol followed by roughly 60 s in methyl isobutyl ketone. Finally, the chip was rinsed in isopropanol. The developers used in this work differ from the commonly used ones [16], however they seemed to work well providing the necessary undercut structure for our purposes.

The evaporation of metal was done in Edwards 306 vacuum coater in a base pressure of $2 \cdot 10^{-6}$ mbar. In order to fabricate superconducting tunnel junctions and resistive environment, three different evaporations were needed. Initially, a thin layer of chromium (8–14 nm) was evaporated at a normal angle. Chromium was chosen, because it has relatively large resistivity and it is easy to evaporate using electron gun. However, too thin Cr layers (less than 6–7 nm) are grainy producing a resistive zero-bias anomaly (Coulomb blockade) in current-voltage characteristics at low temperatures. In order to produce linear current-voltage characteristics, layers thicker than 6–7 nm have to be evaporated. The most resistive Ohmic leads fabricated were of the order of 21 kΩ/μm corresponding to thickness below 10 nm. Usually our 100 nm wide Cr leads had a resistivity of the order of 4–6 kΩ/μm.

After the Cr evaporation the sample was tilted 20 degrees and aluminum (10–20 nm) was thermally evaporated. Because of its favorable properties aluminum is a common choice for superconducting metal. It is easy to evaporate, it can be easily oxidized, and it has a uniform tunnel oxide. Also aluminum has a small grain size compared to the dimensions of our lines (50–100 nm). The critical temperature is $T_c \approx 1.6$ K meaning that temperatures of order 100 mK are needed to measure the quantum properties of our samples.

The first aluminum layer was oxidized by letting about 0.05 mbar of oxygen into the vacuum chamber of the evaporator for about 5 minutes. After oxidation the sample was tilted to -20 degrees and a second electrode was evaporated on top of the first one forming a tunnel junction. Finally, the remaining resist was lifted off in acetone.

As a result of the fabrication process, a single aluminum tunnel junction is connected via high-resistance Cr leads to the soldering pads. Due to the three angle evaporation, each Cr line in the chip has two aluminum satellites on both sides. The tunnel junction is formed between two of these satellites as seen in a scanning electron micrograph of our sample Fig. 6. However, using careful dosage during patterning, the satellites of the Cr lead sections of the sample were evaporated on the sidewalls of the resist and thus removed during lift-off. Otherwise the Al satellites would have shunted the Cr leads destroying the high-resistance environment needed in the measurements.

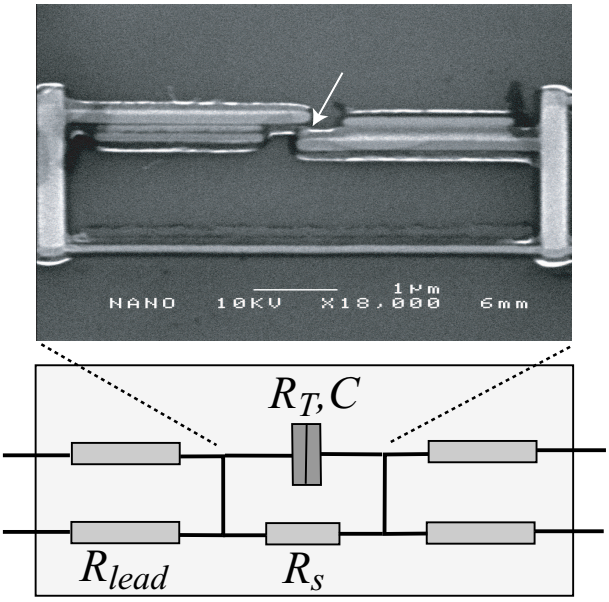

Figure 6: Upper: SEM image of shunted tunnel junction. White arrow shows the position of the overlap junction. The narrow horizontal line is the Cr shunt. Lower: Schematic diagram of the tunnel junction in resistive Cr environment.

2.2 Measurement setup

The samples were attached at the bottom of the mixing chamber of a small plastic dilution refrigerator capable of reaching a base temperature of about 60 mK [18] (see Fig. 7 for the measurement setup). A superconducting 0.5 Tesla magnet was installed outside the vacuum chamber in order to drive the samples into normal state. The cryostat could be cooled from room temperature down to its base temperature within 4 – 5 hours. The sample holder (SH in Fig. 7) at the bottom of the mixing chamber had 12 Thermocoax cables (40 cm long) to bias and measure the sample. These cables also quite effectively filter out the noise from the room temperature electronics [19]. It is important to notice that the sample itself with the resistive Cr leads acts as an effective filter at high frequencies as discussed in Chapter 3.

In the holder, the sample chip was situated in a tight copper enclosure to shield the sample from 4 K radiation of the vacuum chamber. From the sample holder the wires were fed via 1 kΩ resistors, thermalized at 1 K ^{4}He pot of the cryostat. This was also thought to attenuate high-frequency noise from the room temperature electronics.

A home-made [20] preamplifier box (PA) consisting of two instrumentation amplifiers was attached just outside the cryostat body in order to record the voltages across the sample and across a 1 MΩ biasing resistor. This type of preamplifier has also been used

by Delsing *et al.* [21]. The preamplifier box included also a symmetrizer to obtain a symmetric bias $(+V/2, -V/2)$ over the sample. The bias came from a simple op-amp voltage adder which summed DC and AC components provided by two Hewlett-Packard HP33120A function generators.

The voltages were read using HP34401A multimeters (DC part) as well as Stanford SR830 DSP lock-in amplifiers (AC part). The read-out devices as well as the function generators were computer controlled via GPIB bus and the measurement sequence was automated using home-made LabView programs. Typically, using 20 Hz AC excitation and 1 mHz DC sweep due to 1 s integration time in multimeters and lock-in amplifiers, a measurement of a single current-voltage characteristics lasted approximately 17 minutes. However, by streamlining the LabView measurement program and accepting poorer accuracy (smaller integration time) the data acquisition can be made 3-4 times faster.

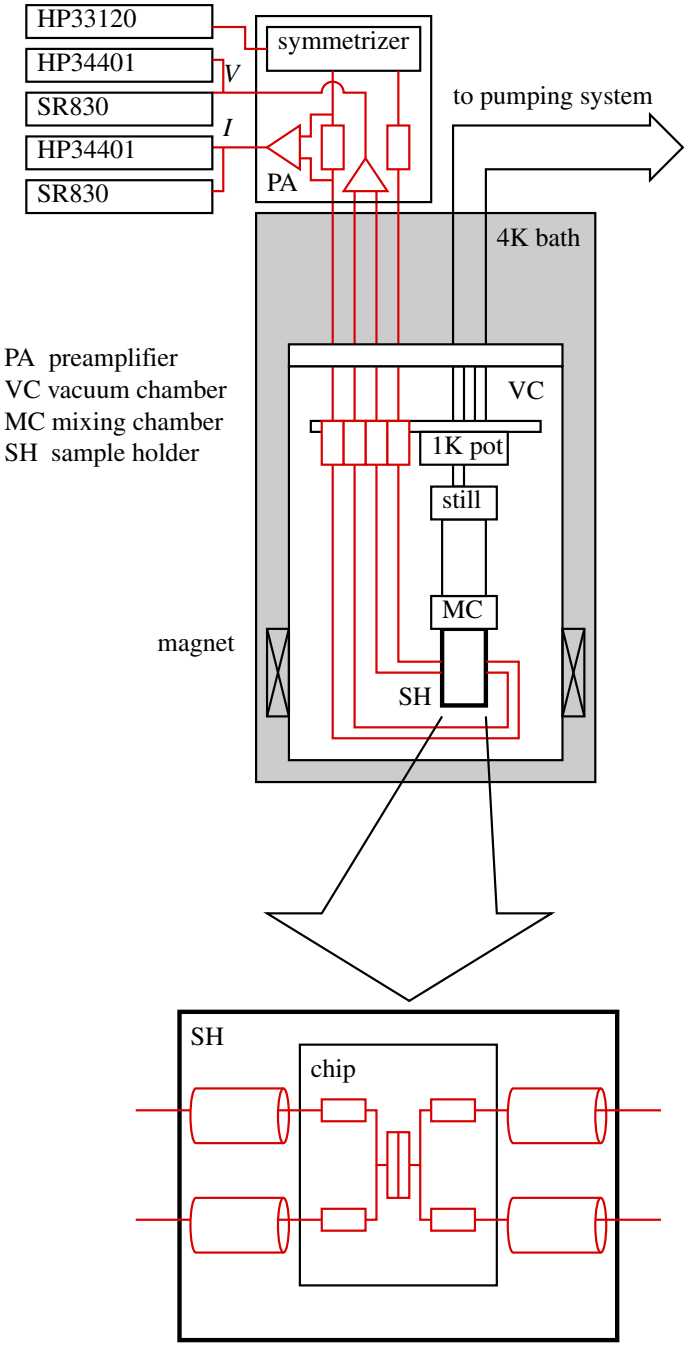

Figure 7: Measurement setup.

The best way to measure the cooling performance of the dilution refrigerator and thus the base temperature of the sample is to attach an on-chip thermometer in the sample holder. A primary Coulomb blockade thermometer [22] can be fabricated using the same process as in the making of the sample. The results yielded a base temperature of 60 mK. The Coulomb blockade thermometer was utilized to calibrate the usual carbon resistor

thermometer used in the actual measurements.

Thermalization of the single electron devices becomes a severe problem at low temperatures. The Joule heating due to current in Cr leads must be transferred to the mixing chamber via the substrate (Fig. 8). The electron-phonon coupling R_{el-ph} in the metal itself is the bottleneck at temperatures in sub-Kelvin range (see [23] and references therein). Kapitza resistance $R_{Kapitza}$ between the phonons in the metal and in the substrate is estimated to be negligible at these temperatures [24].

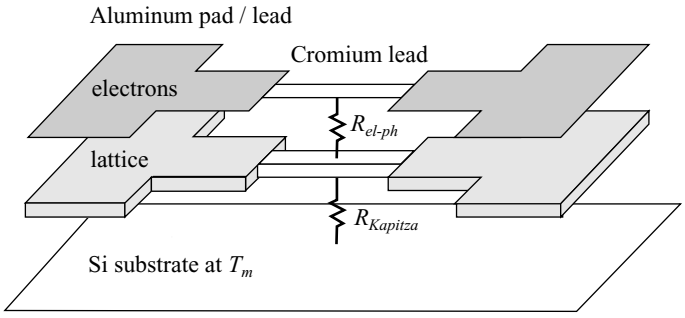

Figure 8: Thermal model of the circuit. Electrons in the chromium leads are coupled to the phonons in the Cr lattice which is in contact with the substrate via Kapitza resistance.

It has been shown [24] that the heat transfer P out of the electron system obeys

$$P = \Sigma\Omega_V(T^5 - T_0^5), \tag{3}$$

where Ω_V is the volume of the shunt and $\Sigma \sim 1$ nW/K$^5/\mu$m^3 is the parameter for electron-phonon coupling. The temperature of the silicon substrate T_0 is assumed to equal the base temperature of the mixing chamber. In Fig. 9, we have equated formula (3) to the dissipated power $R_s I^2$ due to the bias current. Doing so, we also assume that the junction does not conduct, *i.e.* all the current flows through the Cr shunt.

These results suggest that already at relatively low currents the electrons in the Cr shunt ($\rho \sim 1$ kΩ/μm) are heated up well above the practical base temperature of 100 mK. However, the normal metal - superconductor interface between Cr leads and the junction should provide perfect thermal insulation of Josephson junction against hot electrons in the shunt. Thus, despite of finite temperature and possible subgap states in the superconductor, we expect that the temperature of the Josephson junction itself is close to that of the substrate. This is confirmed in P2, where we failed to fit the heating model to measured IV curves.

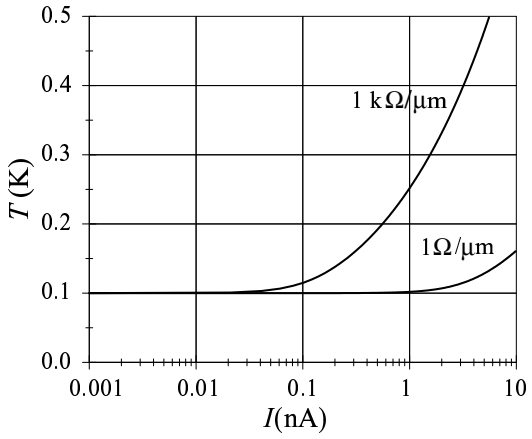

Figure 9: Temperature of the electron system as a function of bias current.

3 Quantum fluctuations in normal tunnel junctions at large voltages

3.1 Effect of environment

In the quantum description of tunnel junction embedded in an environment [13, 25] the junction degrees of freedom Q and φ are coupled to the environmental degrees of freedom, which are represented by an ensemble of harmonic oscillators [26]. These can be viewed as LC-circuits which in the classical limit describe correctly the relaxation of charge according to total impedance $Z(\omega)$. Here

$$\varphi(t) = \frac{e}{\hbar}\int_{-\infty}^{t} dt' V(t') \tag{4}$$

where $V = Q/C$ is the voltage across the junction. This definition becomes more transparent for a Josephson junction where it describes the phase difference of the superconducting condensates (e is replaced by $2e$).

As usual, a Hamiltonian is formed and the tunneling rates are calculated in the limit $R_T \gg R_K$ using the Golden rule. The current-voltage characteristics is given by the difference between forward and backward tunneling rates as

$$I = e[\Gamma^+(V) - \Gamma^-(V)] \; . \tag{5}$$

Integration over the environmental degrees of freedom yields for the tunneling rate [13]

$$\Gamma^+(V) = \frac{1}{e^2 R_T}\int_{-\infty}^{\infty} dE \int_{-\infty}^{\infty} dE' f(E)[1 - f(E')]$$

$$\times \int_{-\infty}^{\infty} \frac{dt}{2\pi\hbar} \exp\left[\frac{it}{\hbar}(E - E' + eV)\right] \langle e^{i\varphi(t)} e^{-i\varphi(0)} \rangle \ , \tag{6}$$

and the backward tunneling rate $\Gamma^-(V) = \Gamma^+(-V)$. Here $f(E)$ is the Fermi distribution, and $\varphi(t)$ is the fluctuation of the phase difference due to fluctuating voltage V across the junction, which is treated as a quantum-mechanical operator. The averaging $\langle ... \rangle$ is performed over possible states of quantum environment. If the phase does not fluctuate, the integral $\int dt$ in Eq. (6) yields the energy delta-function $\delta(E - E' + eV)$, and Eq. (6) reduces to the usual expression for an ohmic tunnel junction. But taking into account the phase fluctuations, Eq. (6) yields (see Eq. (56) in Ref. [13]):

$$\Gamma^+(V) = \frac{1}{e^2 R_T} \int_{-\infty}^{\infty} dE \frac{E}{1 - \exp\left(-\frac{E}{k_B T}\right)} P(eV - E) \ . \tag{7}$$

Here

$$P(E) = \frac{1}{2\pi\hbar} \int_{-\infty}^{\infty} dt \exp\left[J(t) + \frac{iEt}{\hbar}\right] \ , \tag{8}$$

and

$$J(t) = \langle [\varphi(t) - \varphi(0)]\varphi(0) \rangle = 2 \int_{-\infty}^{\infty} \frac{d\omega}{\omega} \frac{\mathrm{Re}Z(\omega)}{R_K} \frac{e^{-i\omega t} - 1}{1 - e^{-\beta\hbar\omega}} \tag{9}$$

is the phase-correlation function where $\beta = 1/k_B T$. Equation (7) includes now all the ingredients to calculate the current-voltage characteristics for a single tunnel junction affected by the environment which is determined as impedance $Z(\omega)$ in Eq. (9).

The asymptotic behavior at $V \to \infty$ is calculated in Ref. [27]:

$$\frac{d^2 I}{dV^2} = \frac{2}{R_T R_K} \frac{\mathrm{Re}Z(eV/\hbar)}{V}. \tag{10}$$

The result does not depend on temperature because $eV \gg k_B T$. The total impedance of the circuit may be presented as $Z^{-1}(\omega) = Y_0(\omega) - i\omega C$, where the admittance $Y_0(\omega)$ refers to the whole circuit except for the capacitive channel C of the tunnel junction. At high frequencies (voltages) one has:

$$\frac{d^2 I}{dV^2} \approx \frac{e^2 R_K}{2\pi^2 C^2 R_T} \frac{\mathrm{Re}Y_0(eV/\hbar)}{V^3} \ . \tag{11}$$

Now integrating twice from V to ∞ we obtain the IV curve

$$I = \frac{1}{R_T} \left[V - \frac{e}{2C} + V_t(V)\right] \ , \tag{12}$$

where the "tail" voltage is

$$V_t = \frac{e^2 R_K}{2\pi^2 C^2} \int_V^{\infty} dV_1 \int_{V_1}^{\infty} dV_2 \frac{\mathrm{Re}Y_0(eV_2/\hbar)}{V_2^3} \ . \tag{13}$$

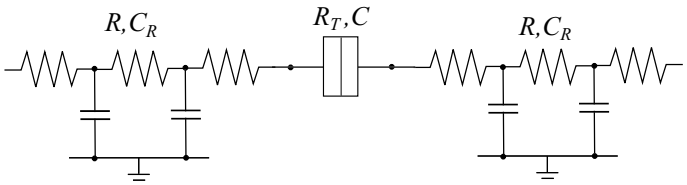

Figure 10: High-frequency model for the measurement setup (see Fig. 6). Cr leads are considered as transmission lines with total capacitance C_R and resistance R.

As seen in Eq. (10) the IV curve at high voltages scans the high-frequency impedance and does not depend on temperature. Thus, only the quantum noise of environment affects the high-voltage behavior. This is manifested by proportionality of high-voltage tails to the quantum resistance R_K. However, the derived asymptotic behavior starts at voltages $V > \pi k_B T/e$ making the observation of asymptotic tails possible only at low temperatures where other masking nonlinear corrections to the junction conductance at required voltages still remain small. Also at large currents the heating of metal by hot electrons (as discussed in Section 2.2) must be taken into account.

3.2 Realistic models for environments

In the case of ohmic environment, $Y_0 = R^{-1}$ and the tail voltage is inversely proportional to applied voltage V as

$$V_t = \frac{R_K}{R}\left(\frac{e}{2\pi C}\right)^2 \frac{1}{V}\ . \tag{14}$$

In a more realistic model the resistors should be considered as transmission lines with distributed resistance, capacitance, and inductance. The admittance of a double transmission line shown in Fig. 10 (drawn without inductive elements) is

$$Y_L(\omega) = \frac{1}{2}\sqrt{\frac{i\omega C_R}{R - i\omega L}}\,\cot\sqrt{i\omega C_R(R - i\omega L)}, \tag{15}$$

where R, L, and C_R are the total resistance, inductance, and capacitance of an individual transmission line. At low frequency ($\omega \ll 1/RC_R,\ R/L$), the admittance becomes purely ohmic, *i.e.*, it behaves as a lumped ohmic resistor: $Y_L \approx 1/2R$.

For a low-resistance transmission line with $R \ll \sqrt{L/C_R}$, the resistance may be neglected, and in the high-frequency limit the double transmission line behaves, nevertheless,

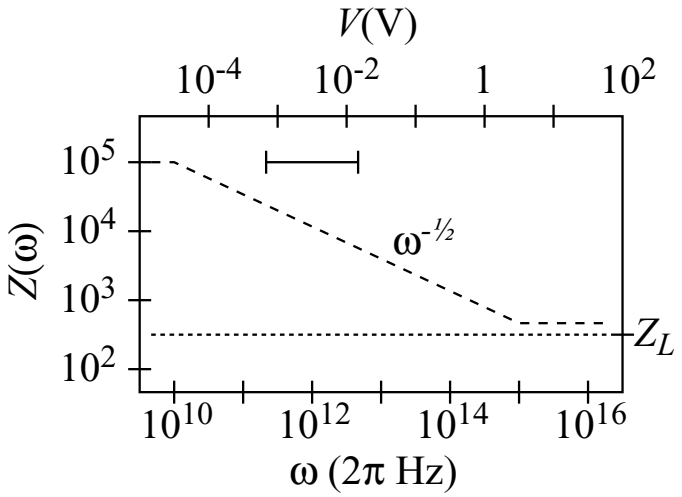

Figure 11: Impedance of transmission line as a function of frequency (voltage) for experimental leads $R = 100$ kΩ and $C_R = 1$ fF (long dashes) and for reference low-impedance line $Z_L \sim 300$ Ω (short dashes). The bar shows the fitting range $\sim$ 1-10 mV. The roll-off frequencies between DC, lossy RC-line and lossless LC-line regimes are $1/RC_R \sim 10^{10}$ Hz and $(R/Z_L)^2(1/RC_R) \sim 10^{15}$ Hz.

as an ohmic resistor with a real impedance $2\sqrt{L/C_R}$ (the energy is lost via radiation along an infinite transmission line). Then the voltage tail is $\propto 1/V$ as for a lumped resistor:

$$V_t = \frac{R_K}{2}\sqrt{\frac{C_R}{L}}\left(\frac{e}{2\pi C}\right)^2 \frac{1}{V} \ . \tag{16}$$

For the high-resistance line with $R \gg \sqrt{L/C_R}$ one may neglect the inductance, and the voltage tail decreases more slowly, as $1/\sqrt{V}$:

$$\begin{aligned} V_t &= \frac{a_{1/2}}{V^{1/2}} \\ a_{1/2} &= \frac{1}{3\pi^{3/2}}\sqrt{\frac{R_K C_R}{RC}}\left(\frac{e}{C}\right)^{3/2} \ . \end{aligned} \tag{17}$$

Irrespective of the magnitude of the dissipative component, at very high frequency $\omega \gg R/L$ (high voltage $V \gg (\hbar/e)R/L$) the (double) transmission line becomes again ohmic with the real impedance $Z_L \approx 2\sqrt{L/C_R}$ which is much smaller than R if the line is long (since R is proportional to the line length, but L/C_R is not). However, if R is large enough, this happens for voltages too high to be relevant in the experiments. The frequency (voltage) dependence of environmental impedance Z is depicted in Fig. 11.

3.3 Horizon model

Alternatively, the voltage tail can be presented as a voltage dependent correction to the junction capacitance:

$$I = \frac{1}{R_T}\left(V - \frac{e}{2\tilde{C}(V)}\right) \tag{18}$$

where the voltage dependent capacitance $\tilde{C}$ becomes

$$\tilde{C}(V) = C\left(1 + \frac{2C}{e}V_t(V)\right) \ . \tag{19}$$

This so-called "horizon model" [28, 29] represents the effect of the environment as due to stray capacitance of leads described by transmission lines. The relevant stray capacitance originates from the length of the transmission line over which an electromagnetic signal from the junction travels during the uncertainty time $\tau_V = \hbar/eV$. This length is called the "horizon" length $v_{ph}\tau_V$, where v_{ph} is the velocity of the signal propagation. Indeed, the effective voltage dependent capacitance incorporating the effect of the voltage tail (see Eq. (19)) can be presented as

$$\tilde{C} = C + c_R v_{ph}\tau_V \ , \tag{20}$$

where $c_R = C_R/\mathcal{L}$ is the capacitance per unit length and $\mathcal{L}$ is the length of the transmission line.

The horizon model was used [28, 29] for lossless (low-resistance) transmission lines where it turns out that

$$\tilde{C} = C + \frac{1}{2\pi^2}\sqrt{\frac{C_R}{L}}\frac{h}{eV} \tag{21}$$

and $v_{ph} = 1/\sqrt{c_R l}$ is of the order of the light velocity (here $l = L/\mathcal{L}$ is the inductance per unit length). But the model works also for lossy (high-resistance) lines where we have

$$\tilde{C} = C + \frac{2}{3\pi^{3/2}}\sqrt{\frac{hC_R}{ReV}} \ . \tag{22}$$

Comparing Eq. (22) with Eq. (20) one sees that $v_{ph} \sim \sqrt{\omega/c_R r} \sim \sqrt{eV\ /\hbar c_R r}$, and is of the order of the phase velocity along the transmission line (here $r = R/\mathcal{L}$). For a lossy line the group velocity of electromagnetic wave is frequency(voltage)-dependent and much less than the speed of light. Thus the horizon picture presents a good qualitative picture of the effect of environment on the high-voltage asymptotics.

3.4 Results

3.4.1 Normal single tunnel junctions

An estimation shows (see caption of Fig. 11) that for the voltage interval studied by us both the leads and the shunt are in the high-voltage regime where they must be

considered as transmission lines. The shunt and leads made from Cr behave as lossy lines and produce an asymptotic square-root law ($1/\sqrt{V}$ -tails). The lines for Al leads and the junction itself are lossless and contribute to the circuit noise as pure ohmic elements (the $1/V$-tail). Thus, both $1/V$- and $1/\sqrt{V}$-tails are present simultaneously in our fitting in high voltage regime ($V > k_BT/e, e/C$) which is based on the formula

$$I = \frac{V}{R_s} + \frac{1}{R_T}\left(V - \frac{e}{2C} + \frac{A_1}{V} + \frac{A_{1/2}}{\sqrt{V}}\right) + gV^3 \ . \tag{23}$$

By introducing a cubic term gV^3 into the fit we take into account the nonlinearity in R_T at large voltages. Even at large voltages ($\sim$10 mV) the strength of the cubic background does not exceed the total contribution from the power law tails. This makes it possible to resolve the power law dependence of the tail. The values of parameters A_1 and $A_{1/2}$ expected from the theory are:

(i) Unshunted junction with low impedance Al leads

$$\begin{aligned} A_1 &= R_K\left(\frac{e}{2\pi C}\right)^2\left(\frac{1}{R_T} + \sqrt{\frac{C_R}{L}}\right), \\ A_{1/2} &= 0 \ . \end{aligned} \tag{24}$$

(ii) Shunted [unshunted] junction with resistive Cr leads

$$\begin{aligned} A_1 &= \frac{R_K}{R_T}\left(\frac{e}{2\pi C}\right)^2 , \\ A_{1/2} &= 3[2]\frac{1}{3\pi^{3/2}}\sqrt{\frac{R_K C_R}{RC}}\left(\frac{e}{C}\right)^{3/2} \ . \end{aligned} \tag{25}$$

The coefficients A_1 include the strong tunneling corrections due to finite $R_T \sim R_K$ by treating R_T like any lumped Ohmic element with $1/V$-tail. The justification of this is presented in P5. The factors 2 and 3 in Eq. (25) appear because four leads are equivalent to two double transmission lines shown in Fig. 10. Thus the total number of double transmission lines is 2 and 3 for the unshunted and the shunted case, respectively. Note that the shunt is considered as two separate sections with resistance $R_s/2$ each. The shunt resistance R_s is known whereas R_T and the capacitance C as well as the parameter A_1 or $A_{1/2}$ are fitted to the IV curve. In the case of lossless Al line (i) the parameter A_1 is fitted freely since it depends not only on R_T, but also on the admittance $\sqrt{C_R/L}$. In the case of Cr leads (ii) A_1 is fixed by R_T and C, and the parameter $A_{1/2}$ is fitted.

In the fabrication process the parameters (electron dose) are equal both for the shunt and the leads. This means that the capacitance and resistance per unit length are equal for Cr shunts and leads. The capacitance per unit length may be estimated from that of a prolate ellipsoid [30]. Using typical values we get $c_R = 100$ aF/μm for our Cr environment. The fit results are compared to theoretical estimates in Table II. Using

the estimated capacitance and the measured resistivity 4 kΩ/μm, one obtains for the attenuation coefficient $\sqrt{\omega r c_R/2} \sim 0.57$ μm^{-1} at 1 mV ($\omega = 1.6 \cdot 10^{12}$ rad/s). Hence, even though our Cr resistors are rather short, they can be viewed practically as infinite.

The Al leads must be characterized by the microstrip impedance [31]

$$\sqrt{l/c_R} = \frac{Z_0}{2\pi\sqrt{\epsilon_{eff}}}\ln(8h/w) \equiv Z_0^{eff}, \tag{26}$$

where Z_0 is the free-space impedance of 377 Ω, $\epsilon_{eff} \sim 6$ is the effective dielectric constant for our silicon substrate, $h \sim 600$ μm is the distance from the ground plane, and $w \sim 200$ nm is the width of the strip. This yields an impedance of 260 Ω.

For presentation, it is convenient to subtract off the linear part $I = V/R_{tot}$ with $R_{tot}^{-1} = R_T^{-1} + R_s^{-1}$. Thus we can plot the "excess" current

$$I_e = V/R_{tot} - I + gV^3 = \frac{1}{R_T}\left(\frac{e}{2C} - \frac{A_1}{V} - \frac{A_{1/2}}{\sqrt{V}}\right) \tag{27}$$

as a function of voltage $V > k_BT/e$.

Figure 12 shows an example of an I_e vs. V-curve measured on a junction with $r = 4$ kΩ/μm Cr leads (sample 3). The best fit is obtained with the lossy RC-line formula of Eq. (17) with $1/\sqrt{V}$-tail. This yields $c_R = 210$ aF/μm for the specific capacitance of the Cr leads, deviating by a factor of two from the estimated value of 100 aF/μm. The results on $1/\sqrt{V}$-tails were found to be independent of temperature in the range 0.1 - 1 K. This is in agreement with theory, according to which the tails depend only on the quantum part of Johnson-Nyquist noise.

Figure 13 shows an I_e vs. V -curve of unshunted sample 2 with thick aluminum leads. As expected, the lossless transmission line formula (24) fits with impedance $\sqrt{L/C_R} \approx$ 570 Ω. This number agrees with Wahlgren *et al.* [28] who calculated R_{env}= 440 Ω from the low-voltage data of a similar unshunted single tunnel junction.

The ratio between the tails A_1/V and $A_{1/2}/\sqrt{V}$ is plotted in the inset of Figure 12. Even though the magnitude $A_{1/2}/\sqrt{V}$ is always larger than A_1/V, their relative magnitude depends on the tunnel resistance R_T. In the strong tunneling regime $R_T < R_K$, A_1/V becomes more dominant than in the samples with larger R_T. This means that one must take strong tunneling effect into account when investigating the high voltage tails, and for this it is sufficient to include the ohmic tunneling resistance R_T into the effective circuit for calculation of the Johnson-Nyquist noise.

Table 2 summarizes the fit results by showing the fitted R_T, C, and the parameter $\sqrt{R_K C_R/RC}$ proportional to the fitting parameter $A_{1/2}$. The theoretical value is obtained from calculated value of capacitance per unit length. The reference sample with lossless Al leads is characterized by the dimensionless impedance $R_K\sqrt{C_R/L}$ comparable to R_K/Z_0^{eff}.

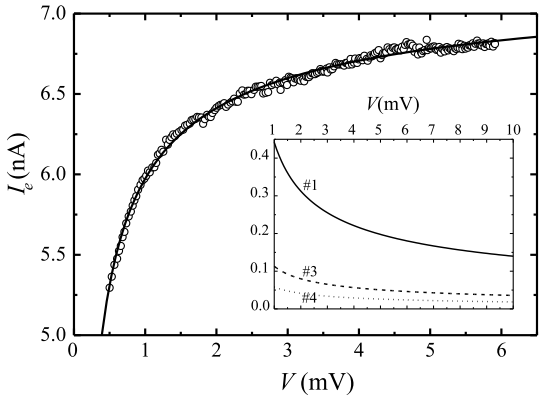

Figure 12: Reduced "excess" current I_e vs. voltage V for sample 3 with tunneling resistance $R_T = 11.1$ kΩ and a resistive 0.1×10 μm^2 Cr shunt ($R_s = 22.4$ kΩ). Solid line illustrates a fit using lossy RC transmission line formulas of Eq. (25). The inset shows the ratio $A_1/V : A_{1/2}/\sqrt{V}$ between two tail contributions arising from tunnel junction and transmission line. The number denotes the sample.

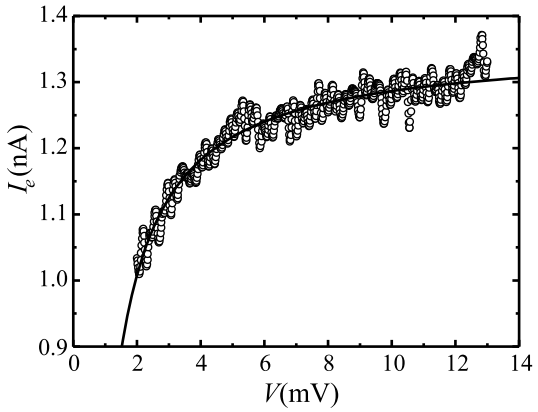

Figure 13: "Excess" current vs. voltage for an unshunted full Al sample with tunneling resistance $R_T = 76.0$ kΩ. The fit has been made using lossless transmission line formulas in Eq. (24).

Table 2: Fit results. R_T and C are fitted to the data. Parameters $\sqrt{R_K C_R/RC}$ and $R_K\sqrt{C_R/L}$ are calculated from the fitting parameters $A_{1/2}$ and A_1, respectively. These are compared with theoretical estimates (see text).

sample	R_T(kΩ)	C(fF)	$\sqrt{R_K C_R/RC}$		R_s(kΩ)	description
			fit	theory		
1	4.3	1.1	1.11	0.77	∞	Cr leads only, $r = 4$ kΩ/μm
3	11.1	1.0	1.16	0.80	22	Cr shunt/leads, $r = 4$kΩ/μm
4	18.4	0.1	3.84	4.15	4.2	Cr shunt/leads, $r = 1.5$kΩ/μm
sample	R_T(kΩ)	C(fF)	$R_K\sqrt{C_R/L}$		R_s	description
			fit	R_K/Z_0^{eff}		
2	76.0	0.7	45.3	99	∞	Al leads only

3.4.2 Nanotubes at large tunneling voltages

As well as metallic samples, the quantum theory of environment can be used to characterize materials with lower carrier concentration like carbon nanotubes [33], where the basic charged excitations are plasmons. IV curves are measured by positioning the nanotube in contact with gold electrodes using a manipulation based on atomic force microscope (AFM) as described in P8. This method produces a double junction geometry, *i.e.* the nanotube acts as a SET island, and a comparison to the environmental theory at high voltages is valid only if the horizon length as described in section 3.3 is less than the length of the nanotube. For our samples, with length about 1 μm, this condition means that the junctions at both ends of the nanotube become independent at voltages larger than a few millivolts. In reality, the junctions are independent already at smaller voltages due to dissipation which attenuates plasmons strongly.

The measurements in P7 reveal a $1/V$ type of high voltage tail corresponding to a resistive environmental impedance of 1.3 – 7.7 kΩ. Relating the value to inductance of Eq. (16) we get $l_Z = 0.1$ – 4.2 nH/μm. The large inductance is due to the large kinetic inductance of low carrier density nanotube.

At low voltages, both Luttinger liquid model (see P7 and references therein) and the quantum theory of environment give the same power law behavior $I \propto V^{\alpha+1}$. Here the exponent can be related to impedance Z by $\alpha = 2Re\{Z\}/R_K$. This yields an inductance $l_\alpha = 0.2$ – 1.7 nH/μm $\approx l_Z$. With the large value of inductance the nanotubes provide an excellent high-impedance environment for a normal junction at high frequencies.

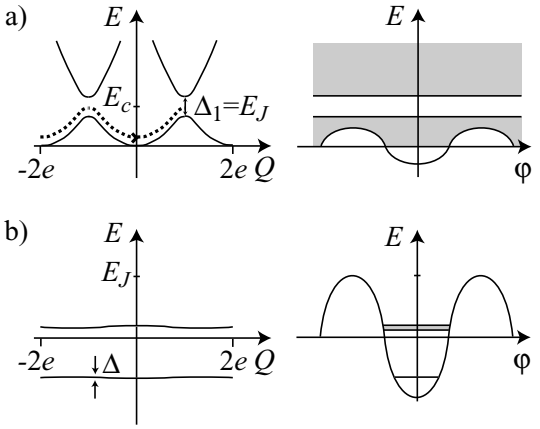

Figure 14: Energy bands for Josephson junction: a) $E_J \ll E_c$, b) $E_J \gg E_c$.

4 Dissipative phase transition

4.1 Band structure of Josephson junction

As already mentioned in Chapter 1, quantum-mechanical tunneling of the phase difference φ causes energy bands to form in the $\cos\varphi$ potential. The limits of weak and strong Josephson coupling are shown in Fig. 14. Analogous to the Bloch electrons, these bands are periodic as a function of quasicharge Q with the period of $2e$. If $E_J/E_c \gg 1$, that corresponds to the tight-binding limit in the solid state theory, then the lowest band is located near $\hbar\omega_p/2$ and given by

$$E(Q) = E(Q+2e) = \Delta[1-\cos(\pi Q/e)] \tag{28}$$

with the band half-width [7]

$$\Delta = \frac{16}{\sqrt{8\pi}}\left(\frac{E_J}{2E_c}\right)^{1/4}\hbar\omega_p \exp\left[-\left(\frac{8E_J}{E_c}\right)^{1/2}\right], \tag{29}$$

where $\omega_p = \sqrt{8E_JE_c}/\hbar$ is the plasma frequency. For a small $Q \ll e$ we may approximate $E(Q) = Q^2/2C^*$ as in the limit of $E_J/E_c \ll 1$ discussed in Chapter 1. Here the effective capacitance $C^* = e^2/\pi^2\Delta$ can exceed the geometric capacitance C essentially.

Now let us shunt the Josephson junction by an Ohmic element R_s. Neglecting interband transitions, the junction dynamics is governed by the band energy $E(Q)$:

$$\begin{aligned} \frac{dQ}{dt} &= I - \frac{V}{R_s} = I - \frac{1}{R_s}\frac{\partial E}{\partial Q} \\ \frac{d\varphi}{dt} &= \frac{2e}{\hbar}V \end{aligned} \tag{30}$$

A stationary solution to Eq. (30) yields Ohm's law $V = R_s I$ at small current bias $I < e/R_s C^*$ corresponding to fixed quasicharge $Q < e$. Here we have used the approximation $E(Q) = Q^2/2C^*$ for the energy band. Physically, all the current flows through the shunt resistor and the Josephson channel is blocked.

However, with increasing current bias the quasicharge approaches the Brillouin-zone boundary ($Q = \pm e$). Then another regime of phase motion sets in [7]: The phase performs Bloch oscillations, with Eq. (30) leading to the period $2e/\bar{I}$, where $\bar{I} = I - \bar{V}/R_s$ is the time average of the current through the junction. In this regime dissipation is suppressed, corresponding to a decreasing resistance V/I.

Thus, at small current bias the resistance must have a bump of width $\delta I = e/R_s C^*$ ($\delta V = e/C^*$), and the shunted Josephson junction behaves as an ohmic resistor with resistance R_s. At larger currents $I \gg e/R_s C^*$, however, the junction has a tendency to become superconducting again. This behavior is a direct outcome of the band picture for the phase motion, as was shown in Ref. [7]. Therefore, a blockade bump in the RI curve of a Josephson junction is a clear manifestation of phase delocalization and the band picture.

The bump on the RI curve at small bias looks similar to the bump due to the Coulomb blockade of single-electron tunneling and, moreover, is governed by a similar effective Coulomb energy $e^2/2C^*$. On the other hand, in the model which we are discussing here, there is no single-electron tunneling at all if the resistance is dominated by the shunt resistance R_s (quasiparticle resistance $R_{qp} \gg R_s$). In fact, we deal with the Coulomb blockade indeed, but it is the Cooper-pair current channel that is blocked [32]. However, in an unshunted junction with $R = R_{qp}$ the additional Coulomb blockade of single-electron tunneling can increase the zero-bias resistance well above R_{qp}.

4.2 Effect of dissipation

The theory as summarized in the previous section would indicate that any Josephson junction must have a blockade bump at zero bias. However, we must take into account an important effect of the environment: suppression of the quantum tunneling by dissipation [5, 34, 35]. This decreases the band half-width which now in the limit $E_J \gg E_c$ is given by

$$\tilde{\Delta} = \Delta \left(\frac{\Delta}{\hbar \omega_p} \right)^{\frac{\alpha_s}{1-\alpha_s}} . \tag{31}$$

Here $\alpha_s = R_q/R_s$ is the dissipation parameter. The renormalized energy $\tilde{\Delta}$ vanishes at $\alpha_s = 1$ where the band disappears. The phase is trapped in some well of the washboard potential and the junction is superconducting down to the lowest current bias. Consequently, the phase line separating insulator from superconductor is the $\alpha_s = 1$ line,

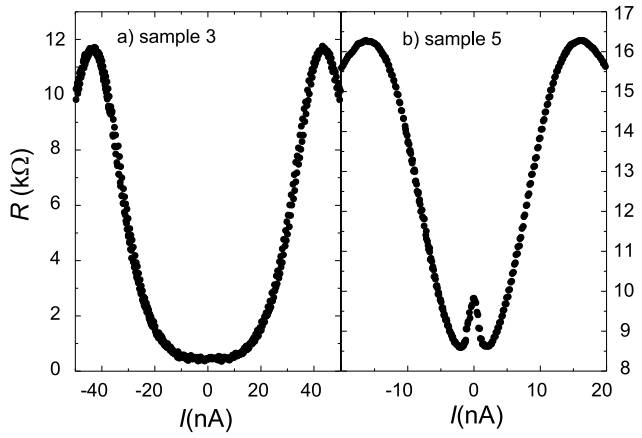

Figure 15: Resistance vs. current for two samples showing different behavior: a) Sample 3 with $R_T = 3.7$ kΩ and $R_s = 11$ kΩ, b) sample 5 with $R_T = 12.4$ kΩ and $R_s = 22$ kΩ.

independent of the energy ratio E_J/E_C (the dashed vertical line on the phase diagram in Fig. 16).

Figure 15 shows two different types of RI curves on both sides of the the dissipative phase transition. On the left, no resistance bump at zero bias is observable, whereas on the right a clear bump is visible.

4.3 Experimental phase diagram

The phase diagram, in which the Josephson junction under weak dissipation remains insulating even in the limit of $E_J/E_C \to \infty$, is difficult to confirm because very slow delocalization of phase leads to exceedingly small voltages. Experimentally, insulating behavior can be observed only if the voltage of the bump, the effective Coulomb gap $e/C^* \sim \tilde{\Delta}/e$, exceeds the minimum voltage V_{min} detectable in our measurements. Therefore, it is reasonable to assume that our measured DPT corresponds not to the condition $\tilde{\Delta} = 0$, but to $\tilde{\Delta} \sim eV_{min}$. Together with Eqs. (29) and (31), the latter condition yields the crossover from the superconductor to the insulator behavior at

$$\frac{E_J}{E_C} = \frac{1}{8}\left(\ln\frac{16}{\sqrt{8\pi}} + (1-\alpha_s)\ln\omega_p\tau_s\right)^2 . \tag{32}$$

Here $\tau_s = \hbar/eV_{min}$ is the phase slip time for the minimum detectable voltage V_{min}. This is the time necessary for a phase change by 2π, *i.e.*, for the phase motion between two wells. In our case, V_{min} is about 0.5 μV which corresponds to $\tau_s \approx 2 \cdot 10^{-9}$ s. The curve obtained from Eq. (32) using $\omega_p = 2 \cdot 10^{11}$ Hz is displayed in Fig. 16. Within

our quite large statistical uncertainty, Eq. (32) agrees with the experimental crossover between superconductor- and blockade-types of RI curves.

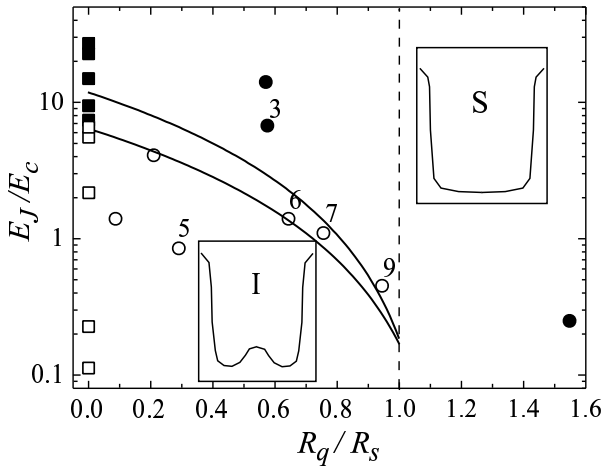

Figure 16: Phase diagram of shunted Josephson junction. The phase boundary lies between insulator-like (open symbols, I) and superconductor-like samples (solid symbols, S). Unshunted samples (squares) are collected at $R_q/R_s = 0$. The solid lines are the theoretical phase boundaries calculated using Eq. (7) with $\omega_p = 2 \cdot 10^{11}$ 1/s and $\tau_s = 2 \cdot 10^{-9}$ s (lower) and $\tau_s = 2 \cdot 10^{-8}$ s (upper).

According to Ref. [7], thermal fluctuations are also able to "wash out" the blockade bump if thermal energy k_BT is of the order of or larger than e^2/C^*. In this case, the crossover is given by Eq. (32) again, but with τ_s replaced by $\hbar/k_BT$ which is about 5 times less than τ_s at our minimum temperature of 50 mK. Since the crossover depends logarithmically on τ_s, small uncertainties in τ_s do not shift its position essentially when compared with our experimental uncertainty. In fact, since the numerical factors in the conditions $k_BT \sim e^2/C^*$ and $V_{min} \sim e/C^*$ are not known, it is difficult to judge which one of these restrictions is stronger.

Table 3: Measured shunted junctions. R_T is deduced from the slope of the normal state IV-curve at high bias voltage. (The effect of parallel shunt R_s is subtracted.) C is calculated from the high bias offset voltage using $V_{\rm offset} = \frac{e}{2C}\frac{R_s}{R_s+R_T}$. The value of R_s is estimated from the known wire resistivity.

sample	$R_T(\mathrm{k}\Omega)$	$C(\mathrm{fF})$	$R_s(\mathrm{k}\Omega)$	E_J/E_c
1	9.7	1.6	75	1.3
2	4.5	2.0	31	3.1
3	3.7	3.2	11	6.2
4	3.4	5.7	11	12.4
5	12.4	1.7	22	0.95
6	8.1	2.1	10	1.7
7	5.9	2.0	8.6	2.5
8	21	0.8	4.2	0.25
9	12	0.7	6.9	0.4

5 Summary

In this Thesis, electron transport through single tunnel junction embedded in a dissipative environment was studied both in normal and superconducting state. High-voltage asymptotics of the IV curves for small normal tunnel junctions and carbon nanotubes were studied experimentally. Power-law voltage tails of IV curve were detected when approaching the linear law $V = IR + e/2C$ at large voltages. The data were in a good agreement with theoretical predictions of the quantum theory of environment (the phase-correlation theory). Despite some numerical-factor discrepancy for high-resistance Cr leads which may be ascribed to inaccuracy of our effective circuit, the voltage tail was observed to grow with increasing lead admittance as predicted by the quantum theory.

Voltage tails of the form $1/V$, typical for low-resistance leads, were experimentally studied and discussed also by Wahlgren *et al.* within the horizon picture [28]. In addition, we detected slower voltage tails $1/\sqrt{V}$ using high-resistance chromium leads. It was shown that the horizon model provides a good qualitative picture also for this type of environment, but only if one takes into account that the high-resistance leads behave as lossy transmission lines in which the electromagnetic signal travels with a frequency-dependent velocity that is much less than the velocity of light.

The effect of environment is in fact a result of Johnson-Nyquist noise in the electric circuit. It is important that the power-law tails at high voltages are connected only with the quantum part of Johnson-Nyquist noise. For the high-voltage tails the condition is $k_BT \ll eV/\pi$ which was well satisfied in our experimental studies. Thus, detection of these tails in a good agreement with theory is a rather unique verification of quantum zero-point fluctuations in macroscopic systems.

Our experimental conditions included the case of strong tunneling when the junction resistance R_T was less than the quantum resistance R_K. The strong-tunneling corrections to the environmental modes at high voltages can be simply incorporated by including the junction resistance R_T into the effective electric circuit for calculation of the quantum noise.

In the superconducting state, our experiments for the first time clearly confirm the existence of the dissipative phase transition in a single Josephson junction, though the observed phase diagram was quite different from that expected originally. The agreement with theory was achieved by taking into account that the position of the measured phase boundary is governed not only by intrinsic junction parameters, but also by the accuracy of voltage measurement. Our work is a strong demonstration of quantum effects in a single Josephson junction, especially, of the Josephson phase delocalization and the band picture of phase motion.

6 Publications

This thesis is based on the following original publications:

DISSIPATIVE PHASE TRANSITION:

P1. J. Penttilä, Ü. Parts, P. Hakonen, M. Paalanen, and E. Sonin, *"Superconductor-Insulator Transition" in a Single Josephson Junction*, Physical Review Letters **82**, 1004 (1999).

P2. J. Penttilä, P. Hakonen, M. Paalanen, and E. Sonin, *Experiments on Dissipative Dynamics of Single Josephson Junctions*, Report TKK-KYL-003 (2001).

P3. J. Penttilä, P. Hakonen, M. Paalanen, Ü. Parts, and E. Sonin, *Dissipative Phase Transition in a Mesoscopic Josephson Junction in a Weak Magnetic Field*, Physica B **284-288**, 1832 (2000).

P4. J. Penttilä, P. Hakonen, M. Paalanen, Ü. Parts, and E. Sonin, *Phase Diagram of Superconductor-Insulator Transition in a Single Josephson Junction*, in *Quantum Physics at Mesoscopic Scale*, Proceedings of the XXXIVth Rencontres de Moriond (EDP Sciences, 2000) p. 345.

IV curves of resistively shunted single Josephson junctions are found to display a crossover between two types of *IV* curves: one without and another with a resistance bump at zero bias. The crossover corresponds to dissipative phase transition at which macroscopic quantum tunneling delocalizes the Josephson phase and destroys superconductivity. The measured phase diagram coincides with the theory that takes into account the accuracy of voltage measurements and thermal fluctuations.

NORMAL TUNNEL JUNCTIONS AT LARGE VOLTAGES:

P5. J. Penttilä, Ü. Parts, P. Hakonen, M. Paalanen, and E. Sonin, *Effect of Quantum Noise on Coulomb Blockade in Normal Tunnel Junctions at High Voltages*, Physical Review B **61**, 10890 (2000).

P6. J. Penttilä, P. Hakonen, M. Paalanen, Ü. Parts, and E. Sonin, *Asymptotic Behavior of a Normal Tunnel Junction at Large Voltages*, Physica B **280**, 399 (2000).

Normal tunnel junctions are investigated at large voltages where even the best Ohmic environments start to look like RC transmission lines. This is manifested by an exceedingly slow approach to the linear behavior above the Coulomb gap. As expected on the basis

of the quantum theory of environment, better fits are obtained using $1/\sqrt{V}$ than $1/V$ dependence for the asymptote. The results agree with the horizon picture if frequency-dependent phase velocity is employed in order to determine the extent of the surroundings seen by the junction.

NANOTUBES:

P7. R. Tarkiainen, M. Ahlskog, J. Penttilä, L. Roschier, M. Paalanen, E. Sonin, and P. Hakonen, *Multiwalled Carbon Nanotubes as High Impedance Transmission Lines*, Report TKK-KYL-004 (2001).

Current-voltage characteristics of multiwalled carbon nanotubes are measured. The transmission line parameters are determined from the high voltage tails. At low voltages, the tunneling conductance obeys non-Ohmic power law in agreement with the predictions of Luttinger liquid and the quantum theory of environment.

P8. L. Roschier, J. Penttilä, M. Martin, P. Hakonen, M. Paalanen, U. Tapper, E. Kauppinen, C. Journet, and P. Bernier, *Single-electron Transistor Made of Multiwalled Carbon Nanotube Using Scanning Probe Manipulation*, Applied Physics Letters **75**, 728 (1999).

In this Paper, a multiwalled carbon nanotube is positioned between two gold electrodes using AFM-based manipulation. The electrical characteristics are investigated using transport measurements.

NOISE:

P9. P. Hakonen, J. Ikonen, Ü. Parts, J. Penttilä, L. Roschier, and M. Paalanen, *Noise of a Single Electron Transistor on a Si_3N_4 Membrane*, Journal of Applied Physics, **86**, 2684 (1999).

The influence of electron-beam writing on the creation of charge trapping centers causing $1/f$ noise is investigated. Two single electron transistors were compared: one where the SET is on silicon wafer covered by a layer of Si_3N_4, and another in which the Si was etched away from below. However, the background charge noise was found to be $10^{-3}e/\sqrt{\mathrm{Hz}}$ at 10 Hz independent of the choice for substrate.

P10. P. Hakonen, M. Kiviranta, J. Penttilä, and M. Paalanen, *Noise Measurements on Single Electron Transistors Using Bias Switching Read-out*, The European Physical Journal Applied Physics, **11**, 227 (2000).

The paper describes a simple bias reversal technique for single electron transistors to remove fluctuations of tunneling resistance from the read-out signal at low frequencies. The gain of the device is kept constant under bias reversal by using asymmetric junction capacitances. In our $Al/AlO_x/Al$ devices with 1.2 μm island size and 100×100 nm^2 tunnel junctions, the noise at 10 Hz is $6{\cdot}10^{-4}e/\sqrt{\mathrm{Hz}}$, independent of the bias modulation.

The author's own contribution:

The research work discussed in this thesis was performed by the NANO group over a time span of four years. It represents a team effort of researchers in different stages of their education. Also contributions by visitors have been invaluable.

I joined the NANO group just after my Masters Thesis in 1995. The first couple of years were spent on literature studies as well as setting up the infrastructure, both sample fabrication line and measurement systems. The first experimental data at mid-1996 was obtained on arrays of aluminum tunnel junctions. The first single junction measurement in tunnel junction environment was carried out just in the end of 1996. The first shunted single junction with strictly Ohmic environment was measured in March 1998.

During the years, I have fabricated samples, prepared experiments, and carried out measurements and data analysis for publications P1-P6. I have been participating in the measurements for publications P7-P10. I have taken part in the writing process of publications P1 and P5 by reading manuscripts, preparing pictures and analysing the final data. Publications P2, P3, P4 and P6 were largely written by myself.

Acknowledgments

First of all, I would like to thank Acad. Olli V. Lounasmaa, the founder of the Low Temperature Laboratory, for originally giving me the chance to work in this excellent laboratory.

I wish to thank Prof. Mikko Paalanen, the present director of the Low Temperature Laboratory, for guiding me into the interesting and new field of nanophysics. I enjoyed learning from him, and I appreciate his invaluable advice, encouragement and patience.

I am grateful to my supervisor Prof. Pertti Hakonen for his dedication and enthusiasm towards complete understanding of everything. I have learned a lot from him. I am indebted to Dr. Ülo Parts for sharing with me the highs and lows of setting up an experimental research facility. Prof. Fred Sharifi provided great help in electron beam lithography. Big thanks to Prof. Edouard Sonin for providing theoretical expertise for our studies.

I was lucky to work with the talented members of the nanogroup, including Markus Ahlskog, Michael Danielides, Jouni Ikonen, René Lindell, Sami Lähteenmäki, Leif Roschier, Paula Routama, Mika Sillanpää, and Reeta Tarkiainen. I wish all of you the best of luck in your future pursuits.

During these years, I have benefitted from discussions with Harry Alles, Alex Babkin, Peter Berglund, Rob Blaauwgeers, Risto Hänninen, Jaakko Koivuniemi, Juha Kopu, Tauno Knuuttila, Juha Martikainen, Kaj Nummila, Jaakko Ruohio, Jussi and Ville Ruutu, Erkki Thuneberg, Viktor Tsepelin, Juha Tuoriniemi, and Janne Viljas.

I should also thank Teija Halme, Marja Holmström, Pirjo Kinanen, Tuire Koivisto, Satu Pakarinen and Liisi Pasanen for keeping the laboratory running. Special thanks to Antti Huvila, Arvi Isomäki, and Antero Salminen for delivering liquid helium for our experiments. Also thanks to the skillful people at the workshop, Juhani Kaasinen, Seppo Kaivola, Hannu Kaukelin, Markku Korhonen, Sami Lehtovuori and Kari Rauhanen, for providing parts to the experimental apparata.

I have not been able to mention all the people with whom I have interacted during my years of research in the laboratory. I hope you forgive me and please accept my gratitude.

Finally, I thank my wife Outi and my parents. They have been an on-going source of encouragement and support.

Otaniemi, January 2001

Jari Penttilä

References

[1] C.A. Neugebauer and M.B. Webb, J. Appl. Phys. **33**, 74 (1962).

[2] H.R. Zeller and I. Giaever, Phys. Rev. **181**, 789 (1969).

[3] J. Lambe and R.C. Jaklevic, Phys. Rev. Lett. **22**, 1371 (1969).

[4] D.V. Averin and K.K. Likharev, in *Mesoscopic Phenomena in Solids*, Eds. B.L. Altshuler, P.A. Lee, and R.A. Webb (Elsevier, Amsterdam, 1991).

[5] G. Schön and A.D. Zaikin, Phys. Rep. **198**, 237 (1990).

[6] *Single Charge Tunneling*, eds. H. Grabert and M.H. Devoret (Plenum Press, New York, 1992).

[7] K.K. Likharev and A.B. Zorin, J. Low Temp Phys. **59**, 347 (1985).

[8] A.N. Cleland, J.M. Schmidt, and J. Clarke, Phys. Rev. Lett. **64**, 1565 (1990).

[9] I.O. Kulik and R.I. Shekhter, Sov. Phys. JETP **41**, 308 (1975).

[10] A. Widom, G. Megaloudis, T.D. Clark, H. Prance, and R.J. Prance, J. Phys. A **15**, 3877 (1982).

[11] P.W. Anderson, in *Lectures in the Many Body Problem* ed. E. Caianello (Academic, New York, 1964).

[12] K.K. Likharev, *Dynamics of Josephson Junctions and Circuits* (Gordon and Breach, New York, 1986).

[13] G.-L. Ingold and Yu.V. Nazarov, Ch.2 in [6].

[14] V.A. Krupenin, D.E. Presnov, A.B. Zorin, and J. Niemeyer, J. Low Temp. Phys. **118** 287 (2000).

[15] G.J. Dolan, Appl. Phys. Lett. **31**, 337 (1977).

[16] M.A. McCord and M.J. Rooks, in *Handbook of Microlithography, Micromachining, and Microfabrication*, Vol. I, Ed. P. Rai-Choudhury (SPIE Press, Bellingham, U.S.A.).

[17] JC Nabity Lithography Systems, P.O. Box 5354, Bozeman, MT 59717 USA. See also www.jcnabity.com.

[18] Nanoway PDR 50, Nanoway Oy, FIN-40500 Jyväskylä, Finland, www.nanoway.fi.

[19] A.B. Zorin, Rev. Sci. Instrum. **66**, 4296 (1995).

[20] S. Lähteenmäki, *Esivahvistin Nanodimensioisten Tunneliliitosten IV-karakterisointiin*, special assignment, Helsinki University of Technology (1997).

[21] P. Delsing, Ph.D. Thesis, Chalmers University of Technology, Gothenburg (1990).

[22] J.P. Pekola, K.P. Hirvi, J.P. Kauppinen, and M.A. Paalanen, Phys. Rev. Lett. **73**, 2903 (1994).

[23] R.L. Kautz, G. Zimmerli, J.M. Martinis, J. Appl. Phys. **73**, 2386 (1993).

[24] M.L. Roukes, M.R. Freeman, R.S. Germain, R.C. Richardson, and M.B. Ketchen, Phys. Rev. Lett. **55**, 422 (1985).

[25] M.H. Devoret, D. Esteve, H. Grabert, G.-L. Ingold, H. Pothier, and C. Urbina, Phys. Rev. Lett. **64**, 1824 (1990).

[26] A.O. Caldeira and A.J. Leggett, Phys. Rev. Lett. **46**, 211 (1981).

[27] D.S. Golubev and A.D. Zaikin, Phys. Rev. B **46**, 10903 (1992).

[28] P. Wahlgren, P. Delsing, and D.B. Haviland, Phys. Rev. B **52**, R2293 (1995); P. Wahlgren, P. Delsing, T. Claeson, and D.B. Haviland, Phys. Rev. B **57**, 2375 (1998).

[29] J.P. Kauppinen and J.P. Pekola, Phys. Rev. Lett., **77** 3889, (1996).

[30] L.D. Landau, E.M. Lifshitz and L.P. Pitaevskii, *Electrodynamics of Continuous Media*, (Pergamon, Oxford, 1984).

[31] See *e.g.* D.M. Pozar, *Microwave Engineering*, 2nd Edition, (John Wiley & Sons, 1998).

[32] D.B. Haviland, L.S. Kuzmin, P. Delsing, and T. Claeson, Europhys. Lett. **16**, 103 (1991).

[33] P.G. Collins and Ph. Avouris, Scientific American, Dec 2000, p. 38.

[34] U. Weiss, *Quantum Dissipative Systems* (World Scientific, Singapore, 1993).

[35] A.J. Leggett, S. Chakravarty, A.T. Dorsey, M.P.A. Fisher, A. Garg, and W. Zwerger, Rev. Mod. Phys. **59**, 1 (1987).